镍基合金焊缝凝固组织演变过程模拟和仿真

马　瑞[1]，　董志波[1]，　魏艳红[1,2]，　占小红[2]
（1. 哈尔滨工业大学 现代焊接生产技术国家重点实验室，哈尔滨　150001；
2. 南京航空航天大学 材料科学与技术学院，南京　210016）

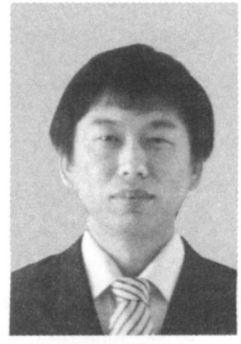
马　瑞

摘　要：建立了一个元胞自动机与有限差分的耦合模型，并将其应用于镍基合金 TIG 焊熔池凝固过程的模拟. 首先对焊接熔池内的各种凝固组织的生长进行了模拟，成功地模拟了平面晶、胞状晶、树枝晶、等轴晶的形态，并与试验结果进行了比照. 进一步模拟熔池凝固时的凝固组织不同形态的演变过程，再现了胞状晶到树枝晶、树枝晶到等轴晶的转变过程. 同时，采用溶质扩散模型模拟了扩散对溶质场分布的影响. 结果表明，模拟结果与试验结果吻合良好.

关键词：焊缝组织演变；元胞自动机法；溶质偏析
中图分类号：TG111.4　　文献标识码：A　　文章编号：0253－360X(2010)07－0043－04

0　序　　言

焊接过程中，焊缝的微观组织对焊接接头的性能有着重要的影响. 焊缝组织形成的过程复杂，受诸多因素影响，而焊缝的一次组织的形成过程在整个焊缝组织演变过程中具有重要意义. 因此，焊缝凝固过程中微观组织演变的研究是一个复杂而重要的领域.

近 20年以来，国内外文献[1－5]利用多种数值计算模型对凝固过程的枝晶生长进行模拟，经历了从晶粒结构到枝晶结构、从二维到三维、从没有流场到包含流场的逐步深入的发展过程[6]，做出了卓有成效的工作. 然而在这些研究中，针对焊接熔池凝固过程的还非常少.

文献[7，8]建立了 CA-FD耦合模型研究分析焊接熔池凝固结晶过程的晶粒形核长大过程. 该模型引入了非平衡扩散理论，并考虑了成分过冷、曲率过冷、动力学过冷等多重过冷度的影响. 计算结果表明，焊接熔池中复杂的温度场和溶质场分布对晶粒生长形态有重要的影响.

文中在上述研究的基础上，基于 CA法对镍基合金焊接熔池凝固过程进行研究，模拟焊缝中各种凝固组织的生长；同时考虑熔池中温度梯度的变化，再现熔池凝固时的组织形态演变过程.

收稿日期：2009－02－26
基金项目：国家自然科学基金资助项目（50775112）

1　模型建立

1.1　溶质扩散模型

溶质扩散对焊接熔池中的枝晶生长具有重要意义，而溶质浓度梯度是溶质在固相以及液相中扩散的驱动力. 固液界面处的溶质浓度集中导致了在固液相中不均匀的溶质场.

在固液界面处，溶质平衡方程为

$$C_S^* = kC_L^* \tag{1}$$

液相溶质扩散控制方程为

$$\frac{\partial C_L}{\partial t} = \frac{\partial}{\partial x}\left[D_L\frac{\partial C_L}{\partial x}\right] + \frac{\partial}{\partial y}\left[D_L\frac{\partial C_L}{\partial y}\right] \tag{2}$$

固相溶质扩散控制方程为

$$\frac{\partial C_S}{\partial t} = \frac{\partial}{\partial x}\left[D_S\frac{\partial C_S}{\partial x}\right] + \frac{\partial}{\partial y}\left[D_S\frac{\partial C_S}{\partial y}\right] \tag{3}$$

式中：C_S^*，C_L^* 分别为固液界面处固相及液相中的溶质浓度；C_S，C_L 分别为固相及液相中的溶质浓度；D_S，D_L 分别为固相及液相中的浓度扩散系数. 在考虑成分过冷和曲率过冷的情况下，有

$$T_{liq}^{\theta} - T_{local} = \Delta T_C + \Delta T_K \tag{4}$$

式中：T_{liq}^{θ}为浓度 C_0 时的液相线温度；T_{local}为局部温度；ΔT_C 和 ΔT_K 分别为成分过冷和曲率过冷. 将 $\Delta T_C = -m_L(C_L^* - C_0)$以及 $\Delta T_K = \Gamma\kappa$代入式(4)，得

$$C_L^* = C_0 - \frac{1}{m_L}(T_{liq}^{\theta} - \Gamma\kappa - T_{local}) \tag{5}$$

式中：m_L为液相线斜率；Γ为 Gibbs-Thomson系数；k为枝晶尖端曲率.

通过式(5)可计算出 C_L^*. 然后通过式(1)~(3),即可得到计算区域内各个位置的 C_L或 C_S.

$$V_x(i,j)=\frac{D_L}{a(1-k)}\left[\left(1-\frac{C_L(i-1,j)}{C_L^*(i,j)}\right)f_L(i-1,j)+\left(1-\frac{C_L(i+1,j)}{C_L^*(i,j)}\right)f_L(i+1,j)\right]+\frac{kD_S}{a(1-k)}\left[\left(1-\frac{C_S(i-1,j)}{kC_S^*(i,j)}\right)f_S(i-1,j)+\left(1-\frac{C_S(i+1,j)}{kC_S^*(i,j)}\right)f_S(i+1,j)\right] \quad (6)$$

1.3 初始条件与边界条件

参考文献[2]的数据,对于镍基合金,模拟所需各种初始参数的设定如表 1所示. 根据表中的公式,元胞自动机时间步取作 0.000 001 s.

表 1 所使用材料的性能和模拟参数

Table 1 Material properties and model parameters used in simulation

液相线温度 T_{LH}/K	液相线斜率 m_L/(K·%)	溶质分配系数 k	液相扩散系数 D_L/(m²·s⁻¹)	固相扩散系数 D_S/(m²·s⁻¹)
1 609	−10.9	0.48	3.0×10^{-9}	3.0×10^{-12}
Gibbs-Thomson系数 Γ/(K·m)	**初始浓度 C_0(%)**	**元胞尺寸 x/μm**	**时间步 t/s**	
1.0×10^{-7}	4.85	5	$\leqslant\frac{1}{5}\min(\frac{\Delta x}{V_{max}},\frac{\Delta x^2}{D_L})$	

2 结果与讨论

2.1 单一凝固组织生长

焊接熔池的凝固组织包括平面晶、胞状晶、树枝晶、等轴晶等结晶形态. 至于具体呈现何种结晶形态,完全取决于结晶期间固—液界面前沿成分过冷的程度[9]. 文中将 1 mm×1 mm的区域划分为 200×200的元胞空间,每个元胞的边长为 5 μm,基于上述模型,对焊接熔池内的各种凝固组织的生长进行模拟. 模拟结果如图 1所示.

2.2 焊缝凝固组织形态演变

为了计算微观区域内的枝晶生长,首先利用商业有限元软件 MARC对 100 mm×50 mm×3 mm的平板构件 TIG焊过程进行宏观温度场的模拟,模拟所用参数为:焊接电压 12 V,焊接电流 160 A,焊接速度 4 mm/s. 计算结果如图 2所示. 取从熔池边缘指向熔池中心的法线路径上的温度分布如图 3所示. 将 1 mm×2 mm的区域划分为 200×400的元胞空间,每个元胞的边长为 5 μm. 底部认为是熔池边缘,而顶部认为是焊缝中心线. 该区域的初始温度场由图 3所示的温度分布差分得到. 降温速率通过熔池中最高温度与熔点温度的差值除以熔池从最高温度到熔点温度所经历的时间获得,文中取为 100 K/s.

1.2 枝晶生长速度模型

在计算枝晶生长速度时,文中采用了 Nastac[3]基于枝晶尖端溶质守恒推导出的枝晶尖端生长速度模型,其公式为

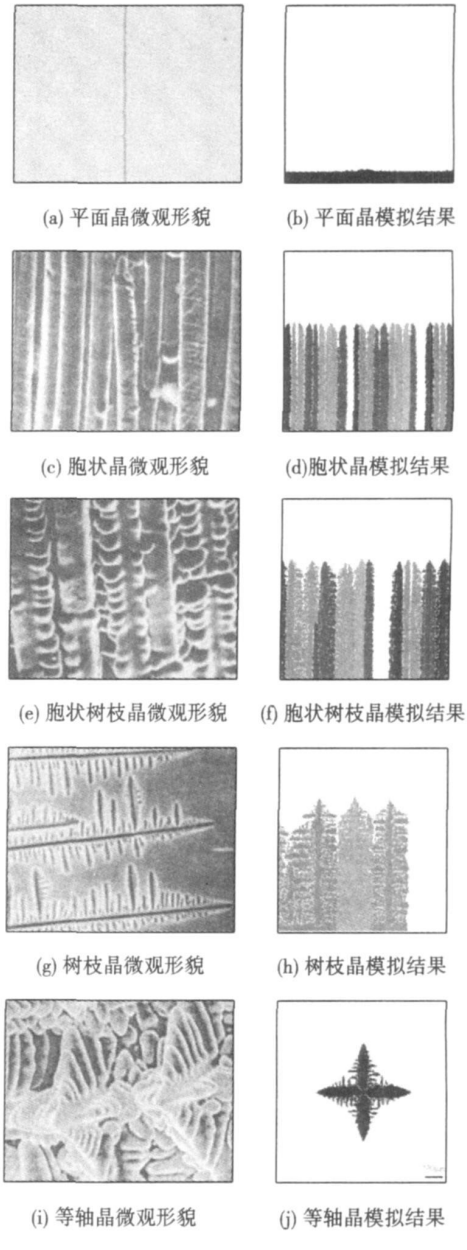

图 1 焊缝中凝固组织形貌比较

Fig. 1 Comparison of dendrite morphologies obtained by experiments and simulations

图 4为熔池内不同时刻枝晶的生长形态. 在结晶的初始阶段,由于熔池边缘的温度梯度较大,同时结晶速度缓慢,此时成分过冷较小,焊接熔池内的枝晶以胞状晶的形式长大. 随晶体逐渐远离焊缝边缘

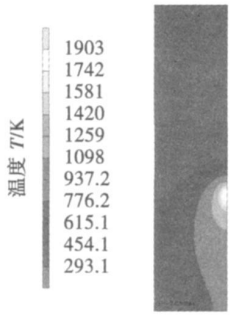

图 2　宏观温度场模拟结果

Fig. 2　Simulated macro temperature field

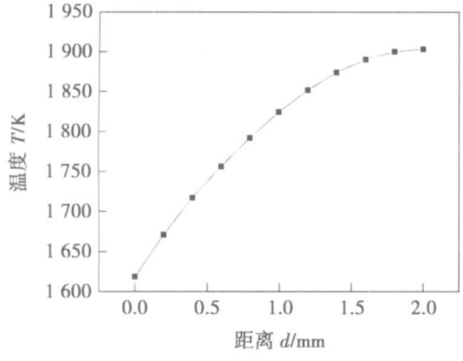

图 3　从熔池边缘指向熔池中心法线路径上温度分布

Fig. 3　Temperature distribution along path from edge of molten pool to center of molten pool

而向焊缝中心生长，温度梯度逐渐减小，结晶速度逐渐增大，成分过冷区也逐渐增大，凸入到过冷液相中的枝晶生长速度更快，阻挡了周围生长速度较慢枝晶的生长，结晶形式由胞状晶向树枝晶转变．而到了凝固后期，在焊缝中心处由于温度梯度最小，成分过冷区最大，在液相中产生新的晶核，以等轴晶的形式长大．在整个凝固过程中，枝晶与枝晶之间、枝晶臂与枝晶臂之间、柱状晶与等轴晶之间都存在着激烈的竞争生长，从而形成了复杂的焊缝金属凝固组织形态．计算结果与图 5所示的试验结果吻合良好．

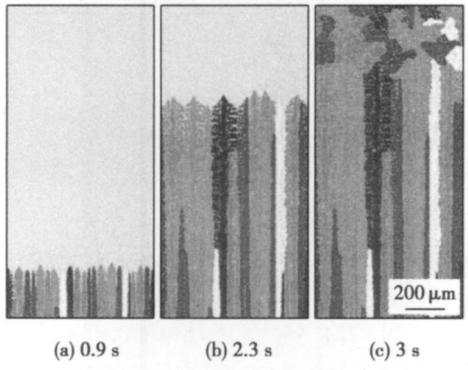

图 4　不同时刻焊缝凝固组织形态

Fig. 4　Simulated dendrite morphologies in molten pool at different times

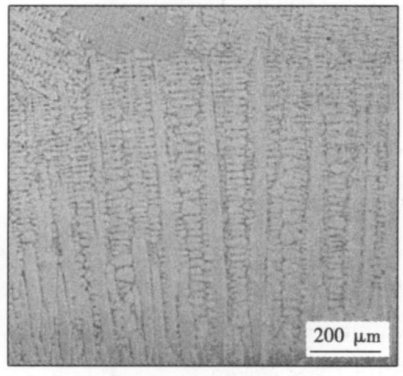

图 5　焊缝组织微观形貌

Fig. 5　Micrograph of molten pool

图 6为图 4在相对应计算条件下不同时刻的溶

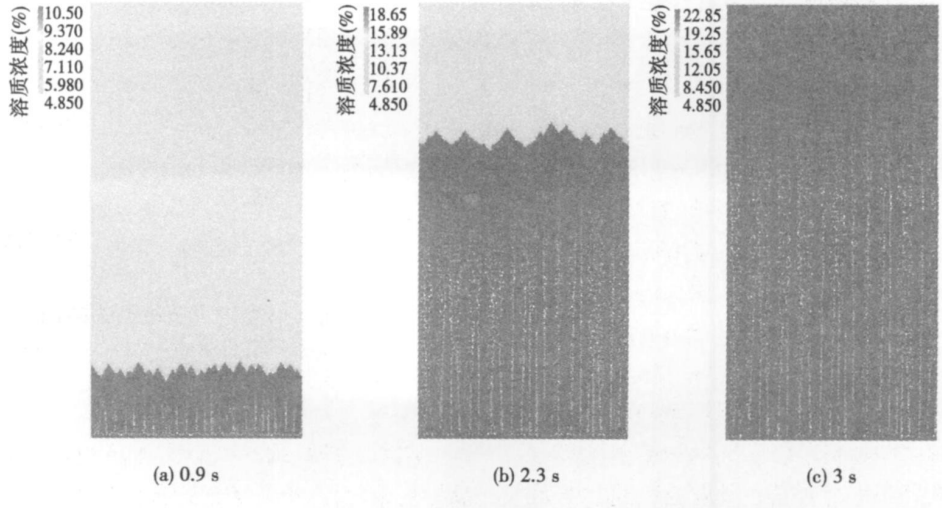

图 6　不同时刻溶质浓度分布

Fig. 6　Simulated solute distribution in molten pool at different times

质浓度分布. 可以看出, 在枝晶前沿以及已凝固区域的残留液相中, 存在溶质堆积现象, 并且随着凝固过程的进行, 溶质堆积不断加剧. 在凝固过程趋于结束时, 液相中的最高浓度达到 22.85%.

3 结 论

(1)建立了一个元胞自动机与有限差分耦合模型, 并将该模型应用于镍基合金焊接熔池的凝固过程模拟.

(2)成功地模拟了焊缝中各种结晶形态, 并与试验结果进行了比照. 进一步模拟熔池凝固时的凝固组织不同形态的演变过程, 模拟结果与试验结果吻合良好.

(3)溶质场的计算结果表明, 随着凝固过程的进行, 溶质堆积不断加剧.

参考文献:

[1] Gandin C A, Rappaz M. A coupled finite element-cellular automaton model for the prediction of dendritic grain structures in solidification processes[J]. Acta Metallurgica, 1994, 42(7): 2233-2246.

[2] Wang W, Lee P D, Mclean M. A model of solidification microstructures in nickel-based superalloys: predicting primary dendrite spacing selection[J]. Acta Materialia, 2003, 51(10): 2971-2987.

[3] Nastac L. Numerical modeling of solidification morphologies and segregation patterns in cast dendritic alloys[J]. Acta Materialia, 1999, 47(17): 4253-4262.

[4] 许庆彦, 柳百成. 采用 Cellular Automaton 法模拟铝合金的微观组织[J]. 中国机械工程, 2001(12): 328-332.
Xu Qingyan, Liu Baicheng. Microstructure simulation of Al alloy with cellular automaton method[J]. China Mechanical Engineering, 2001(12): 328-332.

[5] Zhu M F, Lee S Y, Hong C P. Modified cellular automaton model for the prediction of dendritic growth with melt convection[J]. Physical Review E, 2004, 69(6): 1-12.

[6] 单博炜, 魏 雷, 林 鑫, 等. 采用元胞自动机法模拟凝固微观组织的研究进展[J]. 铸造, 2006, 55(5): 439-443.
Shan Bowei, Wei Lei, Lin Xin, et al. Progresses in numerical simulation of solidification microstructure using cellular automaton method[J]. Foundry, 2006, 55(5): 439-443.

[7] Zhan X H, Dong Z B, Wei Y H. Dendrite grain growth simulation in weld molten pool based on CA-FD model[J]. Crystal Research and Technology, 2008, 43(3): 253-259.

[8] Zhan X H, Wei Y H, Dong Z B. Cellular automaton simulation of grain growth with different orientation angles during solidification process[J]. Journal of Materials Processing Technology, 2008, 208: 1-8.

[9] 刘会杰. 焊接冶金与焊接性[M]. 北京: 机械工业出版社, 2007.

作者简介: 马 瑞, 男, 1983 年出生, 博士研究生. 主要从事焊接过程微观组织模拟及有限元模拟工作. 发表论文 6 篇.
Email: mr0016@sina.com

frequency respond of sound track. Based on the above analysis, the linear generation model of arc sound was set up. The linear prediction coefficients (LPC) $\{a_i\}$, reflection coefficients and logarithm area ratio coefficients were extracted by Levinson-Durbin algorithm. In addition, the combined characteristic vector of arc sound signal was constructed.

Key words: linear prediction analysis; MIG welding; arc sound; feature extraction

Analysis on calculation accuracy and efficiency of multi-pass butt weld of pipe

YU Xingzhe, ZHAO Haiyan, LU Li, LIN Jeanz(1. Department of Mechanical Engineering, Tsinghua University & Key Laboratory for Advanced Manufacturing by Materials Processing Technology, Ministry of Education, Beijing 100084, China; 2. Beijing University of Technology, Beijing 100124, China). p 39—42

Abstract: The influence of segments, heat source and mesh size on calculation accuracy and efficiency of 3-D FEA of multi-pass butt-welded pipe were investigated. The methods can meet the demand of calculation accuracy and high efficiency of 3D finite element simulation of large pipes. The results show that the mesh size below or equals to 3.3mm can meet the accuracy requirement, the segment heat source, which has little efficiencies on calculation accuracy, can improve the calculations efficiency greatly.

Key words: SUS304; multi-pass butt welding; segment heat source; mesh size

Simulation of solidification microstructure evolution in molten pool of nickel base alloy

MA Rui, DONG Zhibo, WEI Yanhong2, ZHAN Xiaohong(1. State Key Laboratory of Advanced Welding Production Technology, Harbin Institute of Technology, Harbin 150001, China; 2. School of Material Science and Technology, Nanjing University of Aeronautics & Astronautics, Nanjing 210016, China). p 43—46

Abstract: A coupled model of cellular automaton and finite difference was established and applied to solidification process in molten pool of nickel base alloy. The growth of various solidification microstructures, including planar crystal, cellular crystal, columnar dendritic crystal and crystal equiaxed dendritic in molten pool was firstly carried out and contrasted with experiment results. Moreover, variation in solidification mode in molten pool was performed, which represented cellular-to-dendritic and columnar-to-equiaxed transitions. The effect of diffusion on the distribution of solute was also calculated by solute diffusion model. The simulation results were in good accordance with the experiment results.

Key words: microstructure evolution; cellular automaton; solute segregation

Microstructural analysis of weld metal microstructures in a low carbon high strength microalloyed steel

WEI Ran, WU Kaiming (Hubei Provincial Key laboratory for System Science on Metallurgical Processing, Wuhan University of Science and Technology, Wuhan 430081, China). p 47—50

Abstract: Microstructural observations and analysis of weld metal in a 800 MPa grade low carbon high strength microalloyed steel are studied by means of potical microscopy, SEM-EDS (Scanning Electron Microscopy-Electron Dispersed Spectrum) and EBBSD (Electron Backscattering Diffraction). The weld metal consists of bainite and acicular ferrite. Acicular ferrite laths or plates are nucleated on inclusions which consisted of an Al_2O_3 core and an outer layer of titanium oxide. Although multi-variant ferrite plates emanate radially from an inclusion, there are only some of them could enlengthen rapidly. It indicates growth direction of acicular ferrite preferred orientation. Results of EBSD analysis also indicate that the acicular ferrite grains in weld metal are not crystallographically oriented randomly, probably a certain orientation relationship being kept. Those acicular ferrite laths or plates nucleated on inclusions grown in opposite direction have the same orientation relationship, presumably because they have a Kurdjumov-Sachs (K-S) orientation relationship with the prior austenite grains.

Key words: high strength low alloy steel; weld metal; acicular ferrite; electron backscattered diffraction

Method of multi-classification by improved binary tree based on SVM for welding defects recongnition

LUO Aimin, SHEN Caihong, YI Bing, LI Kun2(1. School of Light Industry and Food, Sichuan University, Chengdu 610065, China; 2. Luzhou Lao Jiao Co., Ltd., Luzhou 646000, Sichuan, China; 3. School of Electronics and Information Engineering, Sichuan University, Chengdu 610064, China). p 51—54

Abstract: To further recognition accuracy, the multi-classification by improved binary tree based on SVM is raised for welding defects recognition. In the welding defects classification, each class separation is computed, the classes of the two smallest class separation are trained to generate the sub-classification SVM_1 and then are combined into a new cluster G. The new cluster G and the remaining classes are computed similarly and the second sub-classification SVM_2 and new merged cluster H are produced. This work would be repeated until the (k-1)-th sub-classification SVM is obtained and finally a balanced binary tree is come into being. Then, the optimized binary tree based on SVM by clustering is applied in welding defects recognition. The experiments show high recognition accuracy and strong generalization ability by our new algorithm.

Key words: support vector machine; class separation; binary tree; welding defects recognition

A novel high-power inverter-based resistance spot welding power supply

ZENG Min, MA Cheng, CAO Biao, FAN Fengxin (School of Mechanical and Automotive Engineering, South China University of Technology, Guangzhou 510640, China). p 55—58

Abstract: To meet the welding requirements of the new materials with low resistance, a digital powerful medium frequency inverter-based resistance spot welding power is designed, with